Use of FIDAP in sensor and valve optimization problems

J.Maier, S.Stumpf, S.Götz
Robert Bosch GmbH, Department ZWP, D-7000 Stuttgart 10

B.Walz, M.Winter
Computer Centre, Numerics for Supercomputers, University of Stuttgart

Summary:

This paper shows the application of FIDAP to several typical problems in the automotive field for simulating the static and dynamic behaviour of components. The examples dealt with include laminar and turbulent flows as well as heat exchange between gas and solid surfaces.

The example of a high-pressure valve is given to show the capability of FIDAP to calculate turbulent flow patterns in 2D, rotational symmetric geometries. The calculations are carried out on several alternative geometries. In future applications FIDAP may be useful in geometry optimization procedures in this field.

The measurement of air flow may be carried out by using the heat transfer from a sensor surface to the gas, depending on the gas velocity. There ar several requirements to be taken into account for quantitative measurements. They include the knowledge of the local heat transfer depending on the flow patterns near the surface. The range of measurement is usually limited by the onset of non-stationary flow around the sensor. In order to increase this range, the geometry has to be optimized. In this paper we show the calculation of heat transfer for a new sensor concept with different gas velocities. The approach uses FIDAP with a 2D, laminar calculation.

In order to suppress non-stationary flow patterns around a sensor surface calculations were carried out to find out critical parameters including geometry and manufactoring data. The detachment of the flow at a critical angle was extensively studied by fine-mesh techniques using FIDAP on CRAY-II.

In a summary, we try to point out clearly the capabilities and limitations of FIDAP for optimizing and understanding hydraulic and pneumatic components.

Introduction:

The work presented here was carried out by the Bosch Research Department in cooperation with the Computer Centre of the University of Stuttgart. The long-term aim is to introduce CFD techniques into the engineering process in the field of hydraulic and pneumatic components in automotive applications (e. g. sensors and actuators). The part of the work shown in this paper is mainly research work which is not closely related to actual product design. Nevertheless the methods are also used to improve products and to help understand some of the basic flow phenomena.

The main part of our task is to study methods in the field of CFD in order to assist our development branches. Among some other CFD codes we use FIDAP for calculations.

The computers used for the calculations were VAXstations for the pre- and postprocessing and VAXsystems for the calculation. CRAY II of the University of Stuttgart was used for extensive parameter studies as well as for large mesh problems with non-stationary flow. The mesh grids shown in the examples were built with FIMESH. Postprocessing was mainly done with FIPOST. The results were calculated with FIDAP 5.0.

High-pressure valve (example 1):

Problem description:

Figure 1 shows the mesh used to calculate this valve. Valves like this may be used in Diesel equipment. A typical dimension is the diameter of the seat which is approximately 3 mm.

The left side is the high-pressure region with up to 400 bar. A special feature for the calculations was the throttle. The spring of the valve body in the right low pressure part was neglected.

The valve has rotational symmetric geometry. Pressure difference leads to Re numbers of 10 000 to 40 000. Therefore we used a rotationally symmetric model together with k-epsilon turbulence modelling.

The aims of the calculations were to gain insight into typical flow patterns and to try to calculate the body forces which act on the valve contour. With these parameters different geometric variants were studied to get an optimum design regarding flow and force distribution.

Solution procedure:

To simplify matters we used steady state calculations. The required Re numbers were reached with laminar calculations and by increasing Re numbers, which occasionally meant refining the mesh. In this way convergence of the final turbulent calculation was easily achieved.

In a first approach the valve lift was gradually increased from 0.05 to 0.3 mm. Figures 2 and 3 show the results for speed and pressure. At low valve lifts the throttle doesn't play any significant role for the flow whereas for higher lift values the throttle is the dominating feature. Several of the cases show negative pressure values within the valve seat or the inflow of the throttle. In reality fluid will evaporate (cavitation). A distribution of bubbles will result in the flow downstream whereas the pressure will be near zero.

In figure 4 a typical force pattern on the valve contour is displayed schematically. The negative values are due to the negative pressure regions mentioned above. For comparing these values with measurements, they have to be set to zero.

To optimize valve geometry in a first step the angle of the valve seat was varied. Figure 5 shows values from 20° to 40°. The case of reference is shown in the middle (30°). The streamline plot shows typical differences in flow patterns for different angles. The 40°-angle at the bottom reduces the reflection of the flow at the valve body. An analysis of pressure distributions also shows the advantages of this configuration as the negative pressure region is shifted to the upstream direction leading to longer transport distances for bubbles in the flow. This is a fact which may reduce possible damage.

Another way to change the geometry is the modification of the valve body itself. Figure 6 shows the reference geometry with regard to the valve seat region. In figure 7 a somewhat exotic streamlined geometry was modelled.

Figure 8 shows the results for some of these geometry variants from the reference (top) to the streamlined version (bottom). It is evident that the force may be reduced as well as the flow rate increased by the streamlined version. This is a fact which is verified by comparing the forces calculated with FIDAP.

The calculations done so far showed that calculations of turbulent flow in high-pressure valves are feasible. First comparisons with experiments show encouraging results. Nevertheless they have to be looked at critically and more closely. Up to now these calculations played a major part in the development of so-called 1-dimensional models for the valve flow. Models of this kind may be used to simulate the dynamical aspects of hydraulic systems made of several components. In order to derive such models the Bernoulli equation for viscous fluids as well as the momentum equation are used. The use of these equations nevertheless needs the knowledge of the exact flow paths and the locally dependent cross-sections of the flow. The required values were taken from the calculation. For typical classes of valves these models may be universally used.

Air flow sensor, heat transfer (example 2):

Problem description:

In this example we calculate the gas flow around a sensor surface which might be used as an air flow sensor. The sensor is heated to fixed temperature. The heat transfer to the gas depends strongly on temperature difference as well as on gas velocity, therefore the electrical current to keep temperature of the sensor at the same level is an easy measure for the air flow. This is valid with the assumption that the flow is steady or at least periodic.

Sensors using the principle described above are common for measuring air flows. Together with modern technologies these sensors may be reduced in size. In contrast to ceramic plates used in large-scale sensors the contour of such small-scale sensors depends strongly on the technology used.

In the calculation a special membrane structure was assumed where only the thin membrane is heated to temperatures around 160 °C.

We were interested in the velocity region up to 50 m/s, typical values which may occur in the intake part of engines.

The dimensions of the sensor are in the mm-range.

Figure 9 shows the sensor contour together with the grid used in a 2-dimensional laminar calculation including heat conduction in the solid as well as heat transfer between the solid and the gas.

Solution procedure:

A condensed set of results is shown in figure 10 where the mean heat transfer coefficient from solid to gas was plotted against the velocity. The line shows the result from an infinitely large plate, where the heat transfer is proportional to the square root of the velocity. The circles show the upper side of our test sensor. At about 15 m/s flow detachment at the surface occurs. Therefore the heat transfer is reduced fairly below the large-scale limit. The same is true for the lower side where a vortex flow is built up in the etch pit. At velocities higher than 15 m/s the flow pattern is no longer stationary. Therefore the use of the sensor may be restricted to lower velocities as long as the contour is left as calculated.

These calculations were able to show that for small-scale air flow sensors the contour is of much greater importance than in the large-scale area. CFD may help to optimize sensor layout before any measurements on originals have to be done.

Air flow sensor, geometry optimization (example 3):

Problem description:

In this example an air flow sensor made with a common ceramic plate was studied. The sensor is based on a plate with bezels at the front allowing a smoother flow along the plate. Important aspects are the optimization of the sensor geometry with regard to e. g. bezel angles and the systematic study of the influence of production tolerances like small angles of attack.

The mesh used for a 2D-calculation with laminar flow is displayed at the upper picture of figure 11. The fine mesh with more than 16 000 nodes is used to visualize the laminar boundary layer as well as possible detachment processes.

The calculations shown here were part of a project to optimize sensor geometry. The illustrations here deal with the problem of different angles of attack whereas the optimum bezel value of about 20° was found in former calculations.

Solution procedure:

Starting with steady-state calculations the velocity distribution of figure 12 was achieved with an inflow velocity of 1 m/s and a straight alignment of the sensor surface in the flow. There is no detachment at the front and the laminar boundary layer along the sensor is stable (bottom picture).

The picture changes rapidly if the velocity is increased up to 40 m/s where detachment at the front is easily visible (figure 13).

A worst-case analysis with 5°-angle of attack and 5 m/s show detachment of the flow at the downstream edge of the bezels (figure 14). Some millimeters downstream a recirculation zone is build up leading to periodically varying vortices (figure 15). The dimensions of this recirculation zone is shown in figure 16 (bottom) where only regions of negative x-velocity are plotted. The picture at the top gives the non-symmetric pressure distribution in this case.

Calculations were very helpful in this case to obtain the limits of certain parameters which would inhibit correct sensor signals for the air flow. Among them are the angles of bezels as well as the angles of attack. Some other similar parameters of the channel geometry will follow.

Flow detachment from surface (example 4):

The example above was the starting point for a calculation regarding basic flow patterns on a plate and is an a impressive example for the capabilities of FIDAP.

In the case of a fully transient flow with a large angle of attack (5°) and a velocity of 10 m/s a non-stationary calculation was carried out in order to resolve the complex vortex detachment at the surface due to instability of the boundary layer.

The sequences leading to periodic vortex detachment are shown in a video movie which includes the calculations of a 14 h CPU time run at CRAY II based on the 16 000 node mesh of example 3.

This gives a very good impression on the capabilities of today's CFD programs concerning basic research studies.

Outlook:

The four examples we gave of hydraulic and pneumatic components show the use of FIDAP in this context. Our next aim is to intensify the comparison with measurements done on original parts as well as on large models.

This will be an important step towards the introduction of CFD in the engineering environment.

Our main interests in calculation will shift to 2-dimensional turbulent non-stationary problems as well as to complex 3D-geometries. Variable geometries will be dealt with in the near future. For these tasks 3D-UNIX-workstations will be the best suited hardware platform.

Summary:

FIDAP has proved to be a valuable tool for the calculation of fluid flow within hydraulic and pneumatic components. FIDAP calculations soon will become a natural supplement to several measurement techniques using original or enlarged model geometries. In some cases where new principles are to be studied or basic layout alternatives have to be decided calculations will replace the time-consuming and expensive measurements. Up to now the calculations in this field suffer from the lack of a low-Re-number turbulence model which covers the technically important range from Re-numbers of 4000 to 40 000 in a much better way. In order to extend calculation cababilities (e.g. fuel injection components) compressible fluids have to be included in the FIDAP algorithms together with an extension of the Mach number limit to higher values allowing the calculation of critical and overcritical valve flows. These improvements refer mainly to research applications as shown in this paper. In such applications an important aim is to extend FIDAP calculations to much more complex flow patterns. An even more important step for industrial applications is the introduction of FIDAP calculations as a common tool into the engineering process of component development and optimization. Much is left to be done for the so-called "userfriendliness" as well as a speed-up of the calculations perhaps by using modern parallel computing equipment (possibly transputer based). Using standard computing equipment (including supercomputers) FIDAP calculations may contribute in the speed-up of the development process of typical hydraulic or pneumatic components but cannot save much costs. Most of the time a calculation with FIDAP needs is consumed in the preprocessing phase followed by postprocessing including the estimation of the results. Therefore user-friendliness in this part is a strategic aim. User-friendliness in this sense includes mesh generation techniques as well as the integration into CAD-/CAE-environments.

BOSCH ZWP	Valve Optimization with FIDAP	04/91

Mesh for complete valve geometry

Characteristics:

5082 nodal points, 5296 elements
rotational symmetry (2D)
variable valve lift
turbulent calculation (FIDAP 5.03)

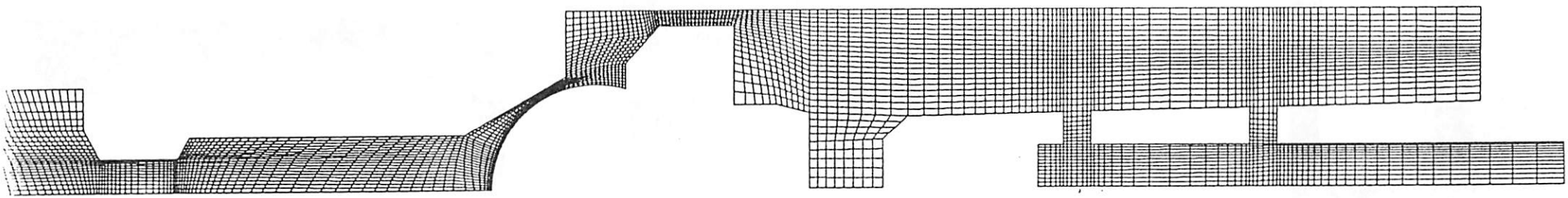

Figure 1:

Mesh for complete high-pressure valve, including low-pressure parts (at right), diameter of valve seat is 3 mm, pressure difference assumed to be 400 bar

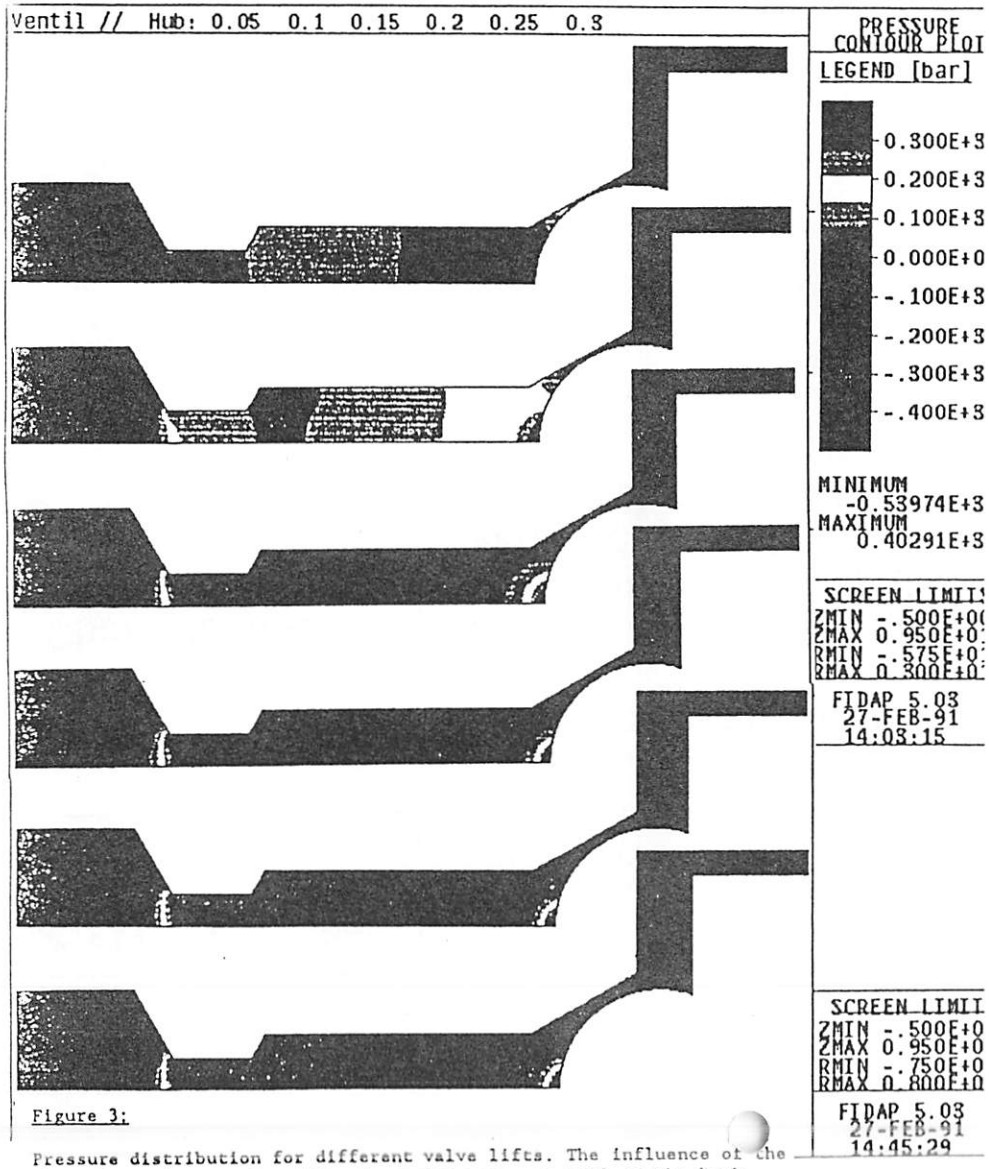

Figure 3:

Pressure distribution for different valve lifts. The influence of the throttle at large valve lifts is easily seen, as well as the back pressure at the center of the valve sphere

BOSCH
ZWP

Valve Optimization
with FIDAP

Tag 04/91

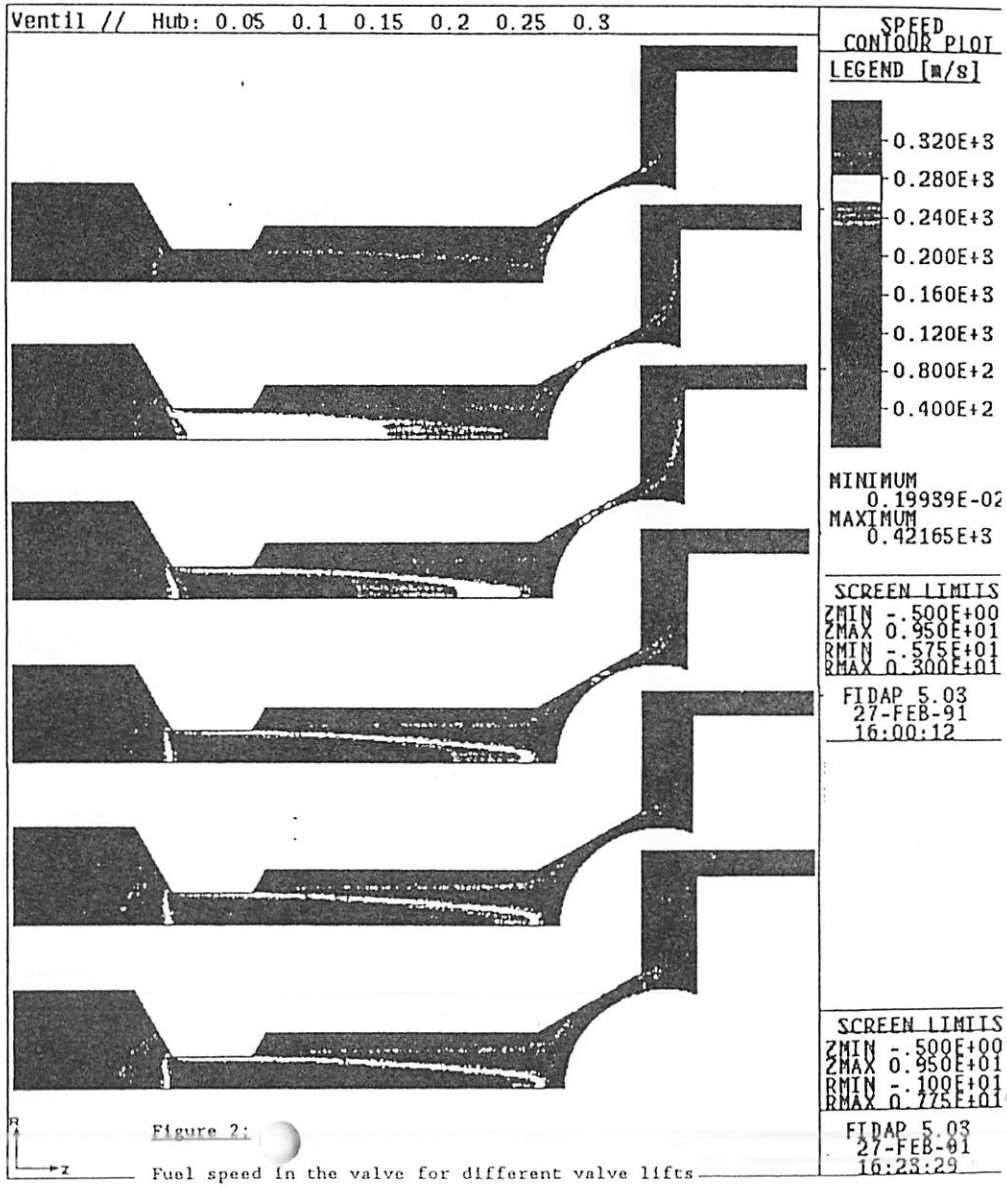

Figure 2:

Fuel speed in the valve for different valve lifts

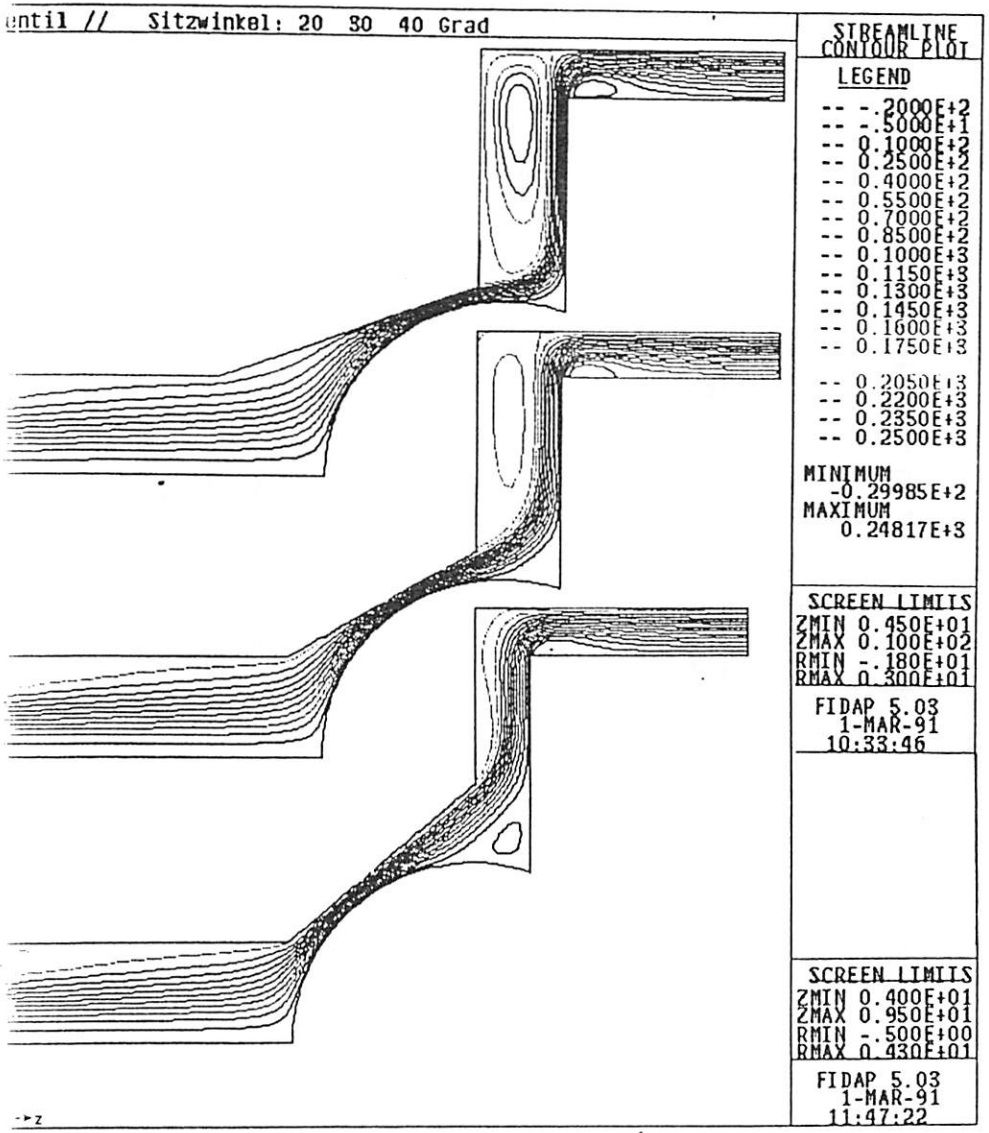

Figure 5:

Influence of different angle values at the valve seat. The picture in the middle gives the reference case of 30 degrees. The differences in

BOSCH
ZWP
Valve Optimization
with FIDAP
Tag 04/91

Force calculations for valve contour

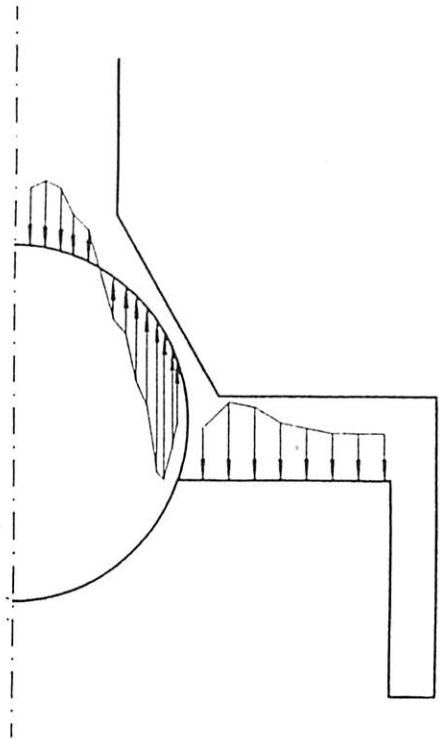

Figure 4:

Typical force distribution at the valve surface, shown for a lift value of 0.2 mm. The negative parts are due to negative pressure along the valve seat. To get reasonable total forces these contributions are set to zero.

Mesh for valve seat studies
Geometry no. 4

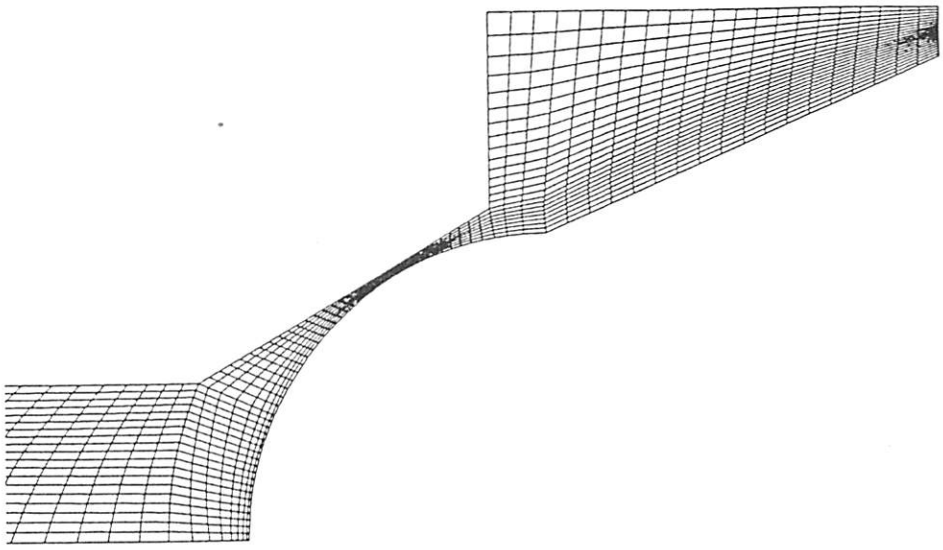

Figure 7:
Mesh for geometry variant with streamlined valve contour

BOSCH
ZWP

Valve Optimization with FIDAP

04/91

Mesh for valve seat studies, reference geometry

Characteristics:

2339 nodal points, 2442 elements
rotational symmetry (2D)
variable valve lift
turbulent calculation (FIDAP 5.03)

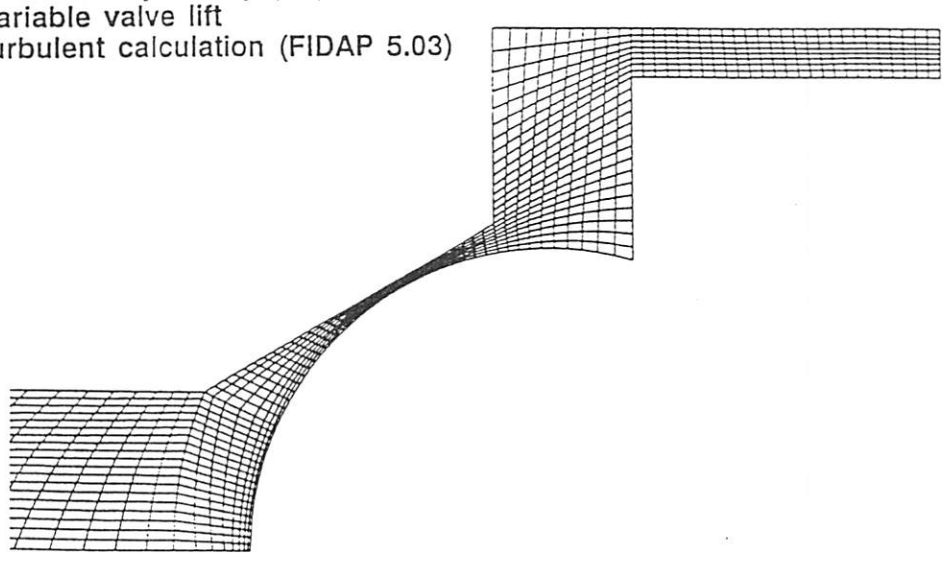

Figure 6:
Enlarged mesh in the seat region for the reference case.

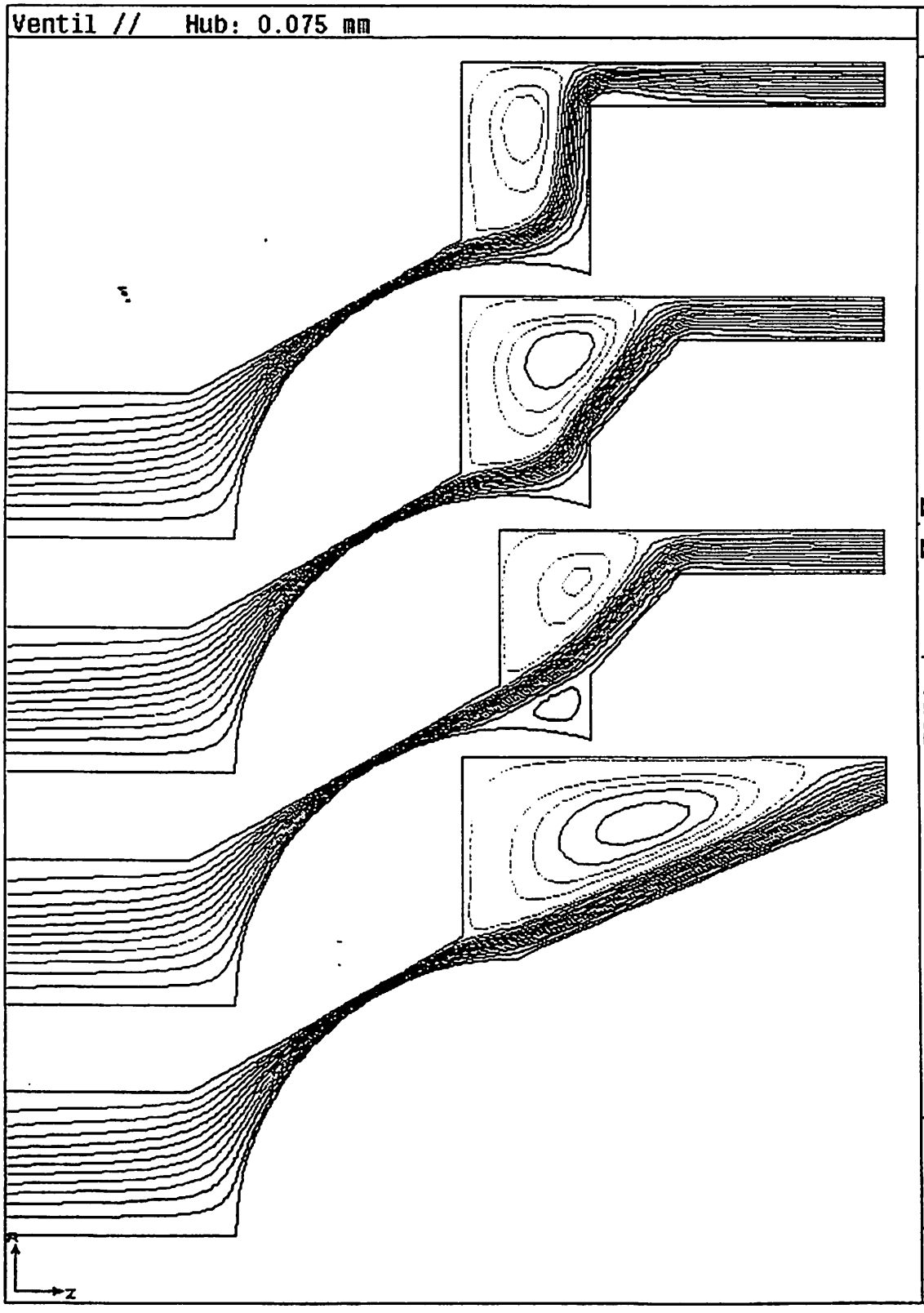

Figure 8:

Streamline patterns for different valve seat geometries at constant lift value of 0.075 mm. The top geometry was the case of reference.

BOSCH ZWP	Heat Transfer Calculations	04/91

Mesh for sensor surface

Characteristics: 5623 nodal points, 1366 elements
2D
laminar calculations, solid elements (thermal conductivity)
heat transfer

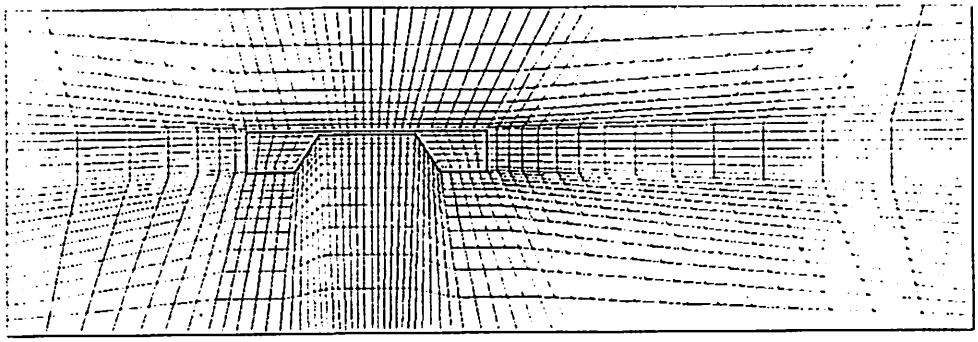

Figure 9:
Mesh for 2D-calculation of air flow sensor. Sensor is built up with solid elements. Sensor dimensions are in the mm-range.

BOSCH ZWP	Heat Transfer Calculations Air Flow Sensor	04/91

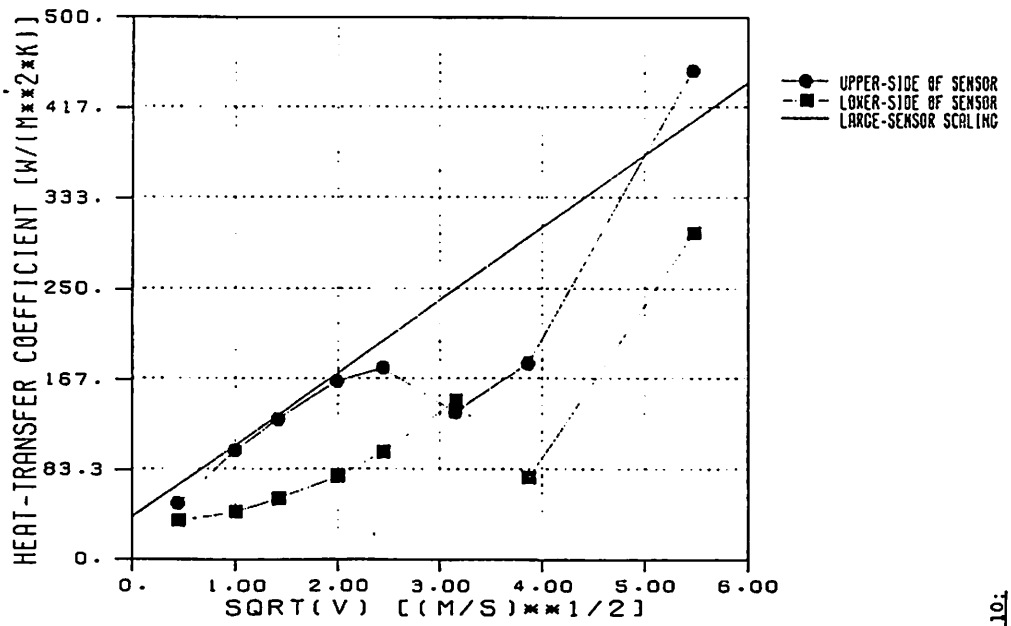

Figure 10:
Calculation of heat transfer coefficients for the sensor surfaces. The squares show the lower side, the circles the upper side. The line gives the theoretical dependency for a large surface. Heat transfer coefficient ist drawn against the square of the velocity.

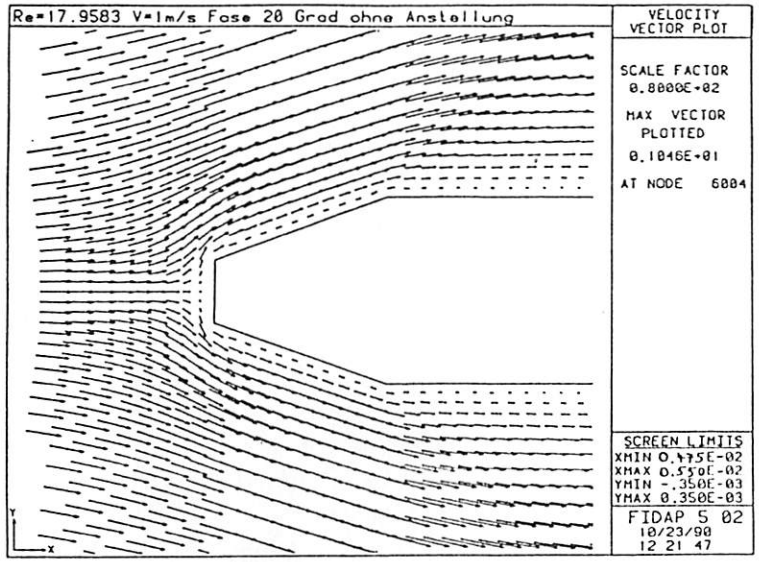

Abbildung 5: Velocity Vector Field

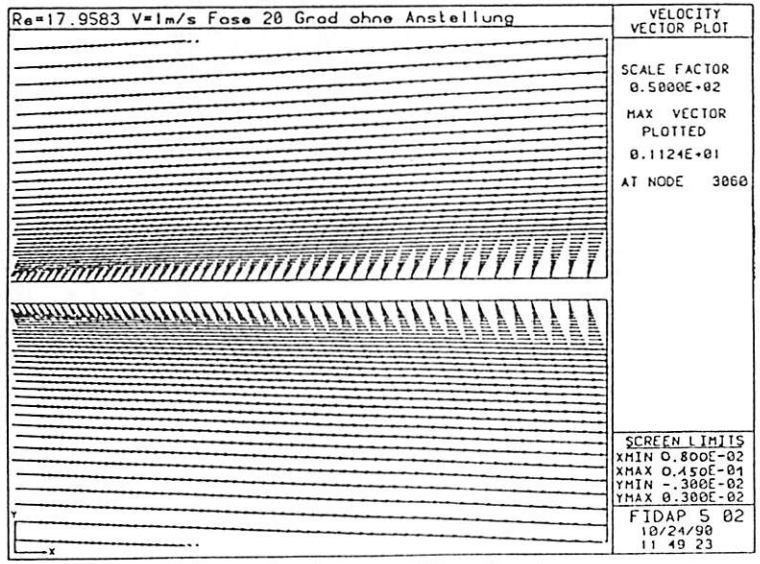

Abbildung 6: Development of Boundary Layer

Figure 12:

Velocity vector plot of front end (top) and surface part (bottom) at 1 m/sec.

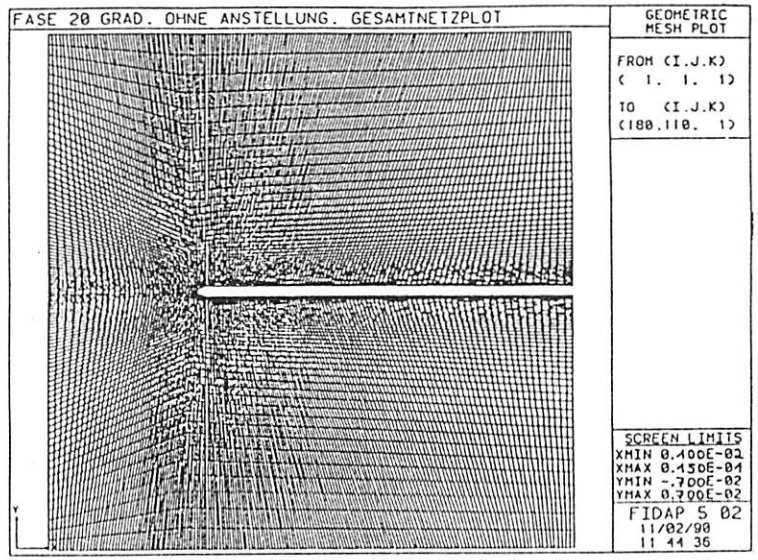

Abbildung 1: Total Mesh Plot

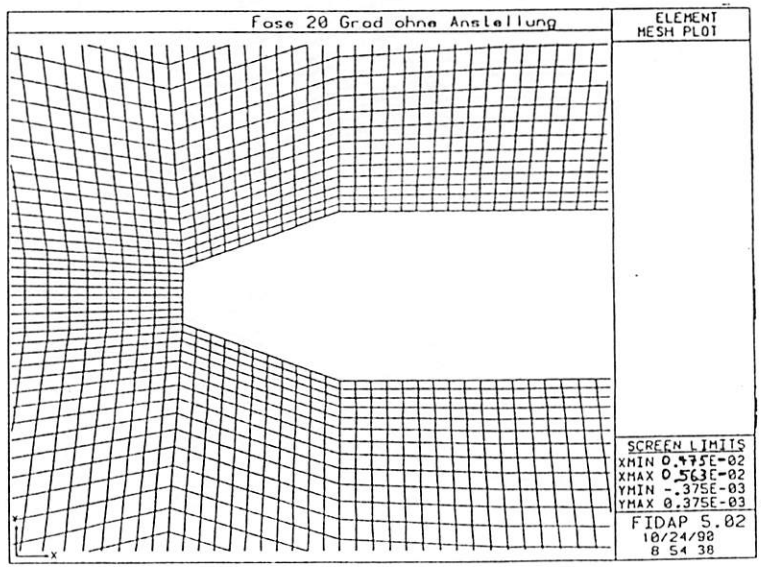

Abbildung 2: Zoom to Front End

Figure 11:

Mesh plots for the surface problem. On the bottom the front region is enlarged. Whole mesh has 16 635 nodes in 2 dimensions.

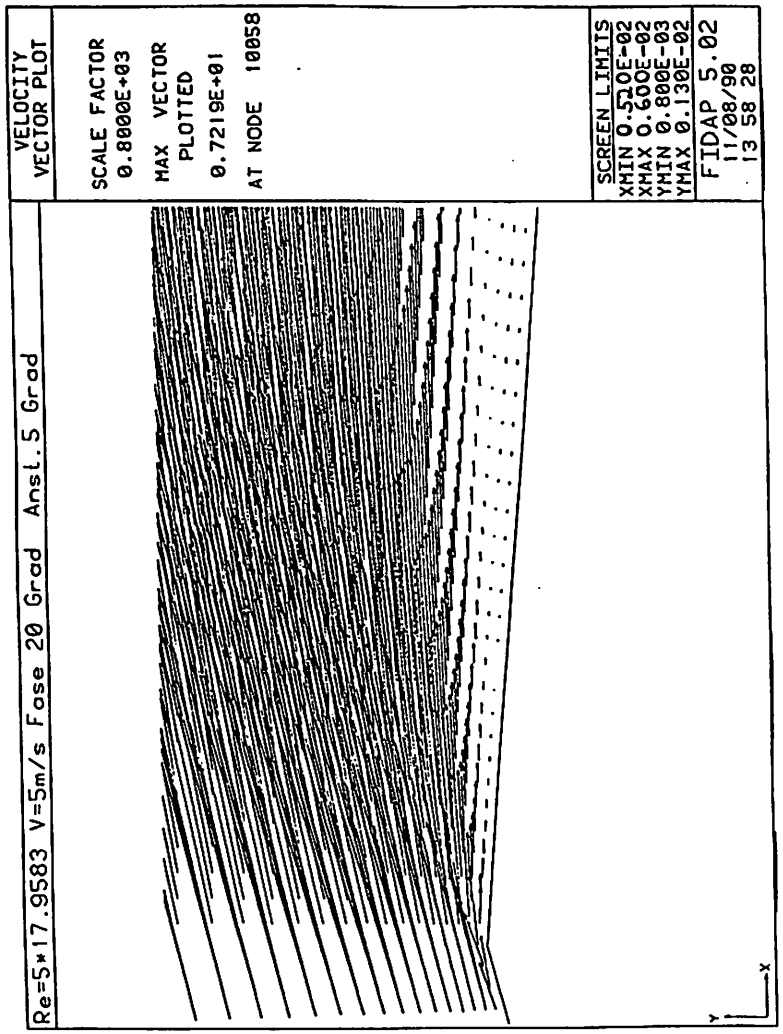

Abbildung 30: Beginning of Separation Bubble, Velocity Vector Field

Figure 14:

Velocity vector plot for 5 m/s, but an angle of att[illegible] of 5 degrees. At the downstream edge of the bezel the detachment i[illegible]een which leads to a reflux region.

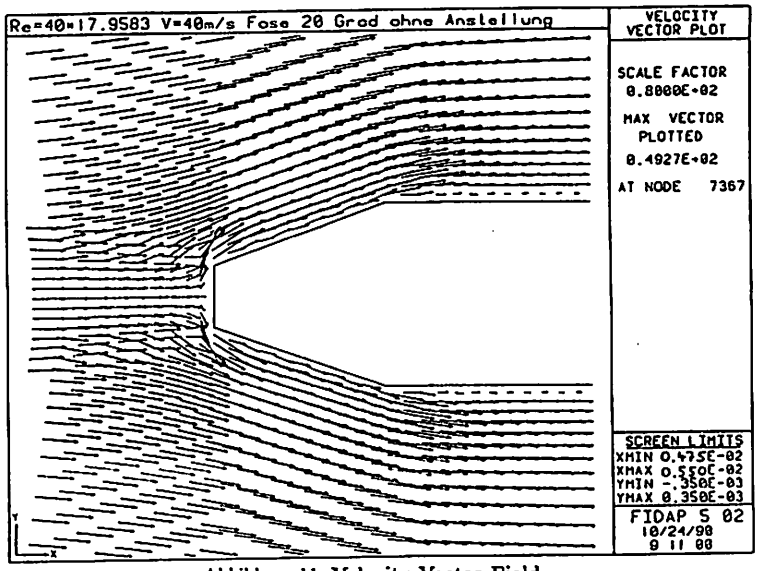

Abbildung 11: Velocity Vector Field

Fig [illegible]11:

Velocity vector plot for 40 m/s, the limit of stationary flow patterns. Detachment of the flow is seen after the bezel range.

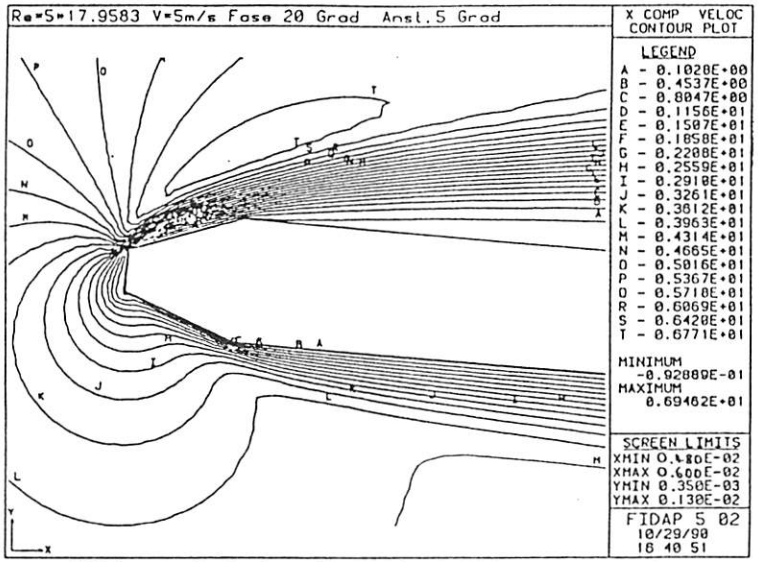

Abbildung 28: Beginning of Separation Bubble, U_x Contour Lines

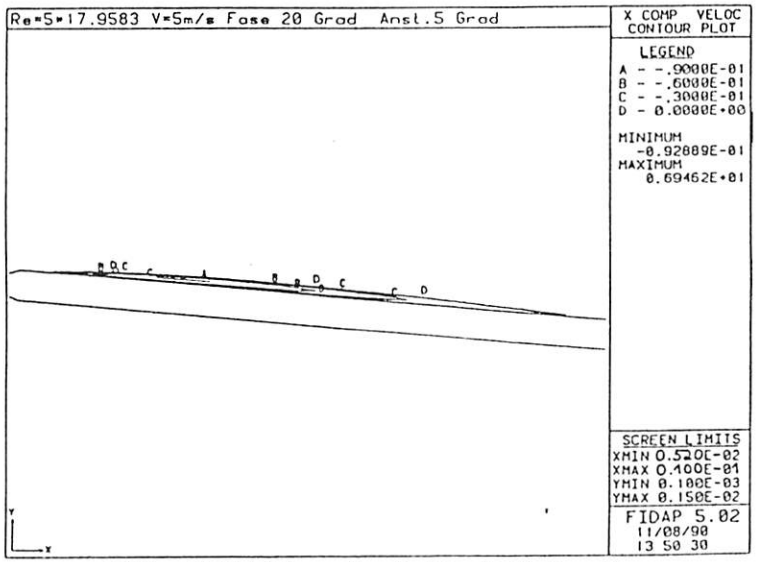

Abbildung 29: Total Separation Bubble, U_x Contour Lines

Figure 16:

Pressure distribution for the case of 5 m/s and 5° angle of attack (top). The picture at the bottom shows the regions with negative

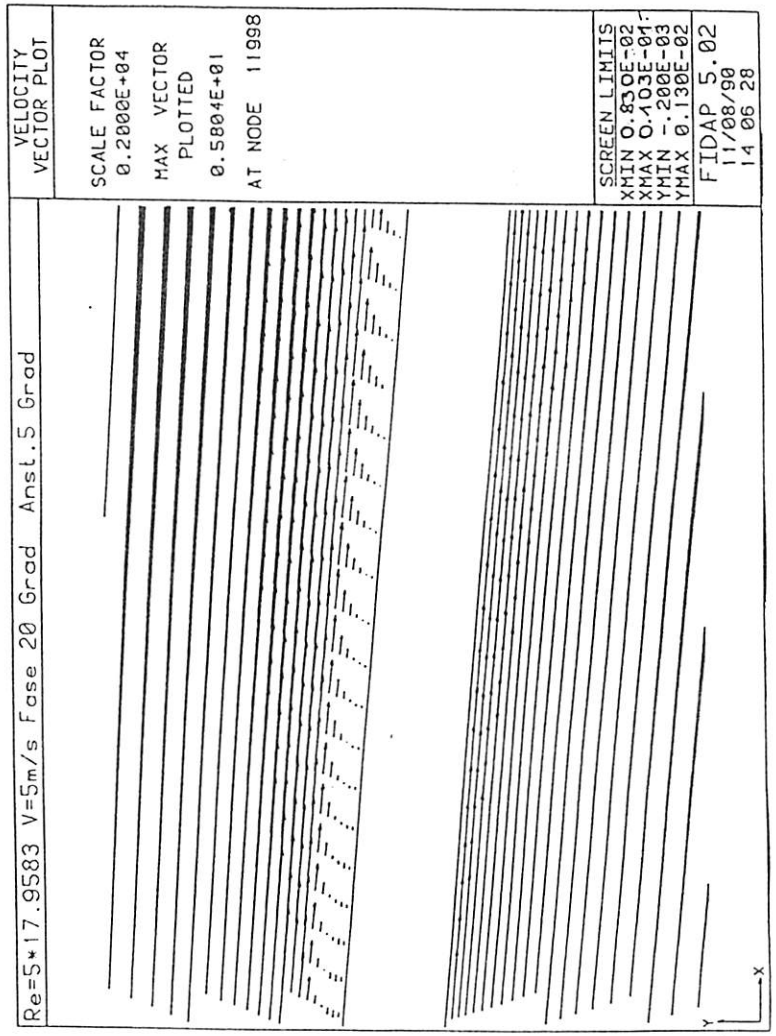

Abbildung 31: Ending of Separation Bubble, Velocity Vector Field

Figure 15:

Reflux region in the middle of the surface at the same conditions as in fig. 14.